



**HAL**  
open science

## Recent progress on ceria doping and shaping strategies for solar thermochemical water and CO<sub>2</sub> splitting cycles

Anita Haeussler, Stéphane Abanades, Julien Jouannaux, Martin Drobek,  
Andre Ayrat, Anne Julbe

### ► To cite this version:

Anita Haeussler, Stéphane Abanades, Julien Jouannaux, Martin Drobek, Andre Ayrat, et al.. Recent progress on ceria doping and shaping strategies for solar thermochemical water and CO<sub>2</sub> splitting cycles. *AIMS Materials Science*, 2019, 6 (5), pp.657-684. 10.3934/matersci.2019.5.657 . hal-02310040

**HAL Id: hal-02310040**

**<https://hal.science/hal-02310040>**

Submitted on 23 Nov 2020

**HAL** is a multi-disciplinary open access archive for the deposit and dissemination of scientific research documents, whether they are published or not. The documents may come from teaching and research institutions in France or abroad, or from public or private research centers.

L'archive ouverte pluridisciplinaire **HAL**, est destinée au dépôt et à la diffusion de documents scientifiques de niveau recherche, publiés ou non, émanant des établissements d'enseignement et de recherche français ou étrangers, des laboratoires publics ou privés.



Distributed under a Creative Commons Attribution 4.0 International License



*Review article*

## Recent progress on ceria doping and shaping strategies for solar thermochemical water and CO<sub>2</sub> splitting cycles

Anita Haeussler<sup>1</sup>, Stéphane Abanades<sup>1\*</sup>, Julien Jouannaux<sup>2</sup>, Martin Drobek<sup>2</sup>, André Ayrat<sup>2</sup> and Anne Julbe<sup>2</sup>

<sup>1</sup> Processes, Materials and Solar Energy Laboratory, CNRS-PROMES, 7 Rue du Four Solaire, 66120 Font-Romeu, France

<sup>2</sup> Institut Européen des Membranes, IEM, UMR-5635, ENSCM, CNRS, Université de Montpellier, Place Eugène Bataillon, Cedex 5, 34095 Montpellier, France

\* **Correspondance:** Email: [stephane.abanades@promes.cnrs.fr](mailto:stephane.abanades@promes.cnrs.fr); Tel: +330468307730.

**Abstract:** Thermochemical redox cycling for either water or CO<sub>2</sub> splitting is a promising strategy to convert solar energy into clean fuels. Such splitting reaction can convert water and recycled CO<sub>2</sub> into H<sub>2</sub> and CO respectively, the building blocks for the preparation of various synthetic liquid fuels. Attractively, CO<sub>2</sub> is valorized in this way and can be used as a carbon-neutral fuel. However, the efficiency of the solar thermochemical process has to be improved to achieve an economically viable fuel production. For this purpose, an optimization of the reactive materials regarding both their chemical activity and long-term stability is a key requirement. To date, ceria is considered as the benchmark material for thermochemical redox cycles. Indeed, it is able to maintain a single cubic fluorite phase during thermal cycling over a large range of oxygen non-stoichiometry and also provides thermodynamically favorable oxidation. However, it suffers from a high reduction temperature and a low reduction extent. Several doping strategies of ceria have been developed to increase its redox activity and long-term performance stability. This paper provides an overview of the efforts made to enhance the thermochemical performance of ceria by investigation of dopant incorporation and material shaping for designed morphologies and microstructures.

**Keywords:** ceria; oxygen vacancies; redox reactions; non-stoichiometric materials; doping; thermochemical cycles; CO<sub>2</sub>/H<sub>2</sub>O splitting; hydrogen; solar fuel

## 1. Introduction

To meet the constantly increasing energy demand while decreasing the carbon footprint induced by fossil fuel combustion, solar energy conversion into high-value clean fuels is considered as a promising solution. The solar energy presents the advantage of being free, largely available and inexhaustible. However, solar energy is also variable, diffuse and intermittent, making difficult its large-scale implementation. Thermochemical cycles for water and CO<sub>2</sub> splitting using concentrated solar power represent a suitable option for solar fuel production without any CO<sub>2</sub> emission. The produced fuel can be stored, transported and used on demand. Thermochemical cycles using non-stoichiometric oxides consist of two steps. The first step is a reduction at high temperature with the creation of oxygen vacancies in the oxide and release of gaseous oxygen (Eq 1). The second step is a re-oxidation reaction of the oxide at lower temperature, resulting in a fuel generation (Eq 2) [1].



Thermochemical cycle operating principle is theoretically simple, although some issues remain challenging, thus impeding industrial implementation. In order to overcome this drawback, numerous studies have been developed to improve the thermochemical performance. To date, the highest solar-to-fuel energy conversion efficiency of 5.25% has been reached with pure ceria as reactive material [2]. To compete with other solar energy conversion pathways such as photovoltaic coupled with electrolysis, the global process efficiency of thermochemical cycles should be over 20% [3]. The main levers to improve the performance of thermochemical cycles are i) development of suitable solar reactor designs, ii) optimization of the operating conditions, and iii) identification of proper reactive materials with both stable redox properties during cycling and optimal shaping and morphology for integration in the solar reactor [3,4]. A suitable reactive material for thermochemical cycles should meet the following criteria: high ability to produce H<sub>2</sub> and/or CO during oxidation, low reduction temperature, rapid reaction kinetics and thermal stability upon redox cycling. Furthermore, the material should be affordable at low costs, non-toxic and largely available [4]. Among the non-stoichiometric oxides, ceria arises as the benchmark material because it exhibits both thermodynamically favorable oxidation and fast oxidation step. However, ceria reduction extent is low, thus impeding high fuel production, which in turn requires high temperatures (in excess of 1400 °C at O<sub>2</sub> partial pressure of 10<sup>-5</sup> atm) to achieve relevant oxygen non-stoichiometry during reduction and substantial fuel production yield during subsequent oxidation. Hence, the required

reduction temperature is generally high, while the maximum process temperature is practically limited because of materials stability issues and heat losses [5–7]. To remedy these problems, two options have been proposed including perovskite oxides as new reactive materials [8–27] and improvement of ceria properties [5–7,28–32]. This article focuses on the recent efforts made to improve ceria performance over the last past years. The optimization of ceria properties via the incorporation of dopants and the relevant shaping strategies are presented in detail.

## 2. Pure ceria as reactive material

Ceria has a cubic fluorite structure with a face centered cubic unit cell ( $Fm\bar{3}m$ ) as represented in Figure 1. The lattice parameter increases linearly with the concentration of  $Ce^{3+}$  due to its larger ionic radius (1.143 Å) than the ionic radius of  $Ce^{4+}$  (0.97 Å) [33,34]. It retains its crystalline phase over a wide range of oxygen non-stoichiometry and reduction extent. The reachable non-stoichiometry depends on both the oxygen partial pressure and the temperature. The Figure 2 shows the influence of temperature and pressure on ceria non-stoichiometry [35–37]. Reduced ceria forms a continuum of oxygen-vacancy in the non-stoichiometric oxide. Due to the non-stoichiometry, there is a distortion of the fluorite structure. Phases with ordered arrangement of the oxygen vacancies have been reported, such as  $Ce_6O_{11}$ ,  $Ce_{11}O_{20}$  and  $Ce_7O_{12}$  [33]. A redox cycle based on the complete thermal reduction of  $CeO_2$  to  $Ce_2O_3$  was first highlighted [38]. A non-stoichiometric partial reduction of  $Ce^{4+}$  to  $Ce^{3+}$  was then performed at lower temperatures [39]. This reaction scheme has been largely studied due to its advantageous combined characteristics such as favorable oxidation thermodynamics, rapid reaction kinetics, complete reversibility and stability. The reduction step of ceria-based thermochemical cycles commonly requires a temperature between 1400 and 1500 °C with an oxygen partial pressure below  $10^{-5}$  atm [7,35,40–42]. Chueh et al. [40] demonstrated stable and fast fuel production over 500 cycles with a solar-to-fuel efficiency in the range 0.7–0.8%. The average  $O_2$  and  $H_2$  production rates over 500 cycles (oxygen partial pressure during the reduction:  $10^{-5}$  atm, reduction and oxidation temperatures: 1500 °C and 800 °C, respectively) are represented in Figure 3. After a decrease of the production rates for both  $O_2$  and  $H_2$  during the first hundred cycles, the average production rates are then stabilized. The authors suggest that the efficiency could be increased by modifying the design and up-scaling, as far as the chemistry was not the limiting step [40]. Furthermore, Chueh and Haile [43] suggest that the solar-to-fuel efficiencies can reach 16 to 19% with an appropriate inert atmosphere during the reduction step [43]. On the contrary, Rager [44] communicated that the efficiency of 0.7–0.8% reported by Chueh et al. [40] was based on the “peak instantaneous efficiency” and that the average efficiency falls to 0.4%. Furthermore, Chueh et al. [40] did not take into account the energy required for producing the purge gas (inert gas recycling) and for the separation of CO from the unconverted  $CO_2$  [44].

Rhodes et al. [45] demonstrated the ability of porous ceria to perform 2000 successive thermochemical cycles (reduction temperature at 1450 °C, oxidation with  $CO_2$  at 1100 °C). The average extent of non-stoichiometry for the last 50 cycles was 86.4% of the average value for the first 50 cycles. The porous structure was maintained in spite of an apparent specific surface area decrease. The obtained mean non-stoichiometry was 0.0197. After repeated cycles, it was observed that the oxidation of ceria tends to be more and more homogeneous through the bulk [45].

Furler et al. [7] also demonstrated the ability of ceria to perform consecutive cycles with stable syngas production.

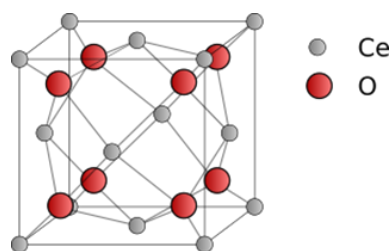


**Figure 1.** Crystalline structure of ceria.

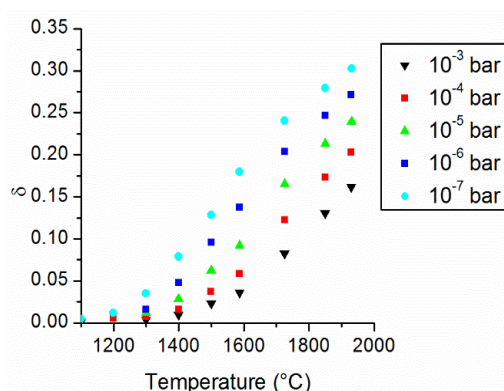


**Figure 2.** Non-stoichiometry in ceria as a function of temperature for different oxygen partial pressures [35].

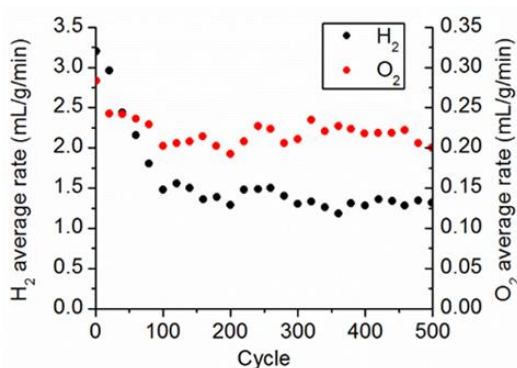


**Figure 3.** Average  $O_2$  and  $H_2$  production rates over 500 successive cycles performed with ceria, reduction temperature of 1500 °C and oxidation temperature of 800 °C [40].

During the oxidation step, bulk oxygen diffusion can be considered as infinitely fast and non-limiting if the diffusion lengths are small [46]. The oxidation is then surface-limited rather than limited by bulk diffusion [43,46,47]. The  $CO_2$  splitting reaction is influenced by, in order of importance, the oxidation temperature and oxidant concentration [48]. Arifin and Weimer [49]

investigated the kinetic mechanisms governing ceria oxidation in thermochemical cycles. They showed that the water splitting reaction follows a first order solid state reaction model (for temperature in the range 750–950 °C and 20–40% H<sub>2</sub>O) and the activation energy is low (29 kJ/mol). In contrast, the CO<sub>2</sub> splitting reaction is a complex surface-mediated reaction [49]. Farooqui et al. [48] studied the kinetics of CO<sub>2</sub> splitting and showed that the general Avrami–Erofeev and Sestak–Berggren models describe well this reaction but the latter fits better for larger range of temperatures and oxidant concentrations [48]. Ackermann et al. [50] investigated the ambipolar diffusion coefficient, which was found to be comprised between  $1.5 \times 10^{-5}$  and  $4 \times 10^{-4}$  cm<sup>2</sup>/s for a temperature from 1400 to 1550 °C. This high value explains the rapid reduction rate of ceria [50].

During isothermal cycles, Davenport et al. [51] showed that H<sub>2</sub> production was only influenced by the gas atmosphere composition and the temperature. Furthermore, higher fuel production can be achieved by splitting CO<sub>2</sub> instead of H<sub>2</sub>O due to the higher oxidizing ability of CO<sub>2</sub> compared with H<sub>2</sub>O in isothermal conditions (at ~1500 °C) [51,52]. The fuel production can be increased by optimizing gas flow parameters and experimental conditions [51]. Ceria has a high entropy change compared to other non-stoichiometric materials, which provides a lower temperature swing requirement between reduction and oxidation. Ceria also provides more favorable oxidation reaction thermodynamics than perovskites [41].

In summary, pure ceria retains a stable fluorite phase over a large range of oxygen vacancy concentration. Furthermore, its re-oxidation is thermodynamically favorable. However, ceria suffers from low reduction extents and thus requires high reduction temperature, limiting the global solar-to-fuel energy conversion efficiency. To overcome these drawbacks, different dopants have been considered to lower the reduction temperature and thus to favor the oxygen release, as presented in the following paragraph.

### 3. Doped ceria

Numerous elements have been incorporated as dopants into ceria trying to both enhance fuel production and decrease the reduction temperature. In order to improve ceria performance by modifying its bulk properties, partial substitution of ceria with aliovalent or isovalent elements was investigated [6].

Meng et al. [51] pointed out that a small ionic radius for divalent, trivalent and tetravalent dopants is beneficial to promote the released amount of oxygen. Furthermore, high valence dopants also enhance the reduction extent. A dopant with high valence and small ionic radius favors the reduction extent of doped ceria. This is due to the Coulombic forces determining the attraction between oxygen-ions and dopant cation, which is proportional to the charges and to the reverse of cation ionic radius. Thus, Ce–O bonds formed around dopants with small ionic radius and high valence tend to break more easily [53].

A summary of the effect of the different doping cations into ceria is given in Table 1. Direct comparison of the cations impact in a quantitative way would not be relevant as it may be biased by strong differences in both operation conditions (reaction temperatures, oxygen partial pressure, gas composition, etc.) and dopant concentrations. Thus, Table 1 rather provides information about the qualitative influence of the cations with positive and negative effects on the reactions.

**Table 1.** Summary of cations effect on the reduction extent, fuel production and thermal stability.

|                          | Cation           | Reduction extent | Fuel production | Thermal stability |
|--------------------------|------------------|------------------|-----------------|-------------------|
| Monovalent               | Li <sup>+</sup>  | +                | +               |                   |
| Divalent                 | Ca <sup>2+</sup> | -                |                 |                   |
|                          | Cu <sup>2+</sup> | +                | ≈               |                   |
|                          | Mg <sup>2+</sup> | +                | +               | ++                |
|                          | Sr <sup>2+</sup> | -                |                 |                   |
| Trivalent                | Co <sup>3+</sup> | ++               | -               | --                |
|                          | Dy <sup>3+</sup> | ≈                | -               | +                 |
|                          | Er <sup>3+</sup> | +                | -               | -                 |
|                          | Gd <sup>3+</sup> | -                | -               |                   |
|                          | La <sup>3+</sup> | +                | ≈               |                   |
|                          | Nd <sup>3+</sup> | -                | -               | +                 |
|                          | Pr <sup>3+</sup> | +                | -               |                   |
|                          | Sc <sup>3+</sup> | +                | +               | +                 |
|                          | Sm <sup>3+</sup> | +                | ≈               |                   |
|                          | Tb <sup>3+</sup> | +                | +               | -                 |
|                          | Y <sup>3+</sup>  | -                | -               |                   |
| Tetravalent              | Cr <sup>4+</sup> | +                | ≈               |                   |
|                          | Ge <sup>4+</sup> | +                |                 |                   |
|                          | Hf <sup>4+</sup> | +                | +               | -                 |
|                          | Rh <sup>4+</sup> | +                |                 | --                |
|                          | Si <sup>4+</sup> | +                | -               | -                 |
|                          | Sn <sup>4+</sup> | ++               | -               |                   |
|                          | Ti <sup>4+</sup> | +                | -               |                   |
|                          | Zr <sup>4+</sup> | ++               | -               | -                 |
| Pentavalent              | Nb <sup>5+</sup> | +                | -               |                   |
|                          | Ta <sup>5+</sup> | +                | +               | -                 |
|                          | V <sup>5+</sup>  | -                | -               | -                 |
| Multiple oxidation state | Fe               | ++               |                 |                   |
|                          | Mn               | ++               | -               | -                 |
|                          | Ni               | ≈                | ≈               |                   |
|                          | Zn               | +                | +               |                   |

\*Note: Symbols “+”, “-” and “≈” represent an increase, decrease and no significant variation of the properties due to the cation addition compared with pure ceria, respectively.

### 3.1. Monovalent dopant

Meng et al. [54] studied the effect of monovalent Li<sup>+</sup> ion on ceria thermochemical performance. They showed that up to a dopant concentration of 5% Li (atomic composition), the amount of produced oxygen increased. Conversely, maximum H<sub>2</sub> production was obtained for the minimum Li concentration tested (2.5%). However, the authors did not compare Li-doped ceria to pure ceria. Therefore, it is necessary to remain cautious when reporting that 2.5% of Li may increase the H<sub>2</sub> production in comparison with pristine CeO<sub>2</sub>. The reduction step follows a second-order reaction

mechanism for a temperature in the range 1000–1170 °C (with an activation energy  $E_a = 44.4$  kJ/mol for  $Ce_{0.95}Li_{0.05}O_2$ ), whereas for a temperature in the range 1170–1500 °C the reaction mechanism follows a contracting–cylinder model (with  $E_a = 86.6$  kJ/mol for  $Ce_{0.95}Li_{0.05}O_2$ ). Indeed, diffusion lengths are small in the low temperature range, so the diffusion is fast. In contrast, diffusion lengths are larger due to sintering in the high temperature range, making the diffusion through the grain slower. Thus, the change in the solid-state model can be caused by sintering which increases the powder grain size [54].

### 3.2. Divalent dopants

Kaneko et al. [28] highlighted that Cu dopant in ceria improved  $O_2$  release compared with pure ceria due to a partial reduction of Cu species from Cu(I) to Cu(0). However,  $Cu_2O$  does not take part during the oxidation step. Hence,  $H_2$  production from Cu-doped ceria is similar to pure ceria performance [28], and the addition of Cu dopant in ceria does not provide any beneficial interest for the improvement of the solar-to-fuel efficiency.

The effect of cerium substitution with strontium and calcium on thermochemical performance was also studied [53,55]. It appears that the amount of  $O_2$  released by  $Ce_{0.9}Sr_{0.1}O_2$  is slightly lower than with  $CeO_2$ . Similarly, the reduction extent of  $Ce_{0.9}Ca_{0.9}O_2$  is lower than for pure  $CeO_2$ . It is noteworthy that Sr-doped ceria was expected to produce lower oxygen amount than Ca-doped ceria due to the larger ionic radius of  $Sr^{2+}$  than  $Ca^{2+}$ . This finding can be explained by the higher thermal stability of Sr-doped ceria compared to Ca-doped ceria [53]. The second O-vacancy formation energy for Ca- and Sr-doped ceria are comparable to the value for undoped ceria, thus explaining the similar behavior of Ca- and Sr-doped ceria compared to pure ceria [56]. These results were confirmed by Scheffe and Steinfeld [55] who stated that Ca- and Sr-incorporation into  $CeO_2$  did not improve the solar-to-fuel energy conversion efficiency.

The use of the  $Mg^{2+}$  ion as dopant in ceria increases the  $O_2$  production yield (1.98 mL/g) at 1500 °C in comparison to pure ceria (1.77 mL/g). The bulk conductivity of ceria is improved by the increase of the oxygen vacancy concentration due to the incorporation of  $Mg^{2+}$  cation. The lower valence state of  $Mg^{2+}$  compared to  $Ce^{4+}$  leads to an increase in the amount of intrinsic oxygen vacancies. During the oxidation step at 500 °C under steam water, the magnesium dopant also permits to enhance the  $H_2$  production and re-oxidation yield (3.89 mL/g and 1.97 mL/g, respectively) compared with pure ceria (3.19 mL/g and 1.80 mL/g, respectively). Moreover,  $Ce_{0.9}Mg_{0.1}O_2$  presents a good stability over cycles with a  $H_2$  production of 3.85 mL/g during the 2<sup>nd</sup> cycle and 3.81 mL/g during the 9<sup>th</sup> cycle [53]. However, the solubility of  $Mg^{2+}$  is limited due to the important difference between the ionic radii of  $Ce^{4+}$  and  $Mg^{2+}$ , 0.97 Å and 0.89 Å, respectively [57].

### 3.3. Trivalent dopants

The influence of scandium as a dopant in ceria is shown in Figure 4 [59]. The introduction of Sc in ceria is limited to 20 at.%. The small ionic radius of  $Sc^{3+}$  compared to  $Ce^{3+}$  permits to relieve the lattice strain induced by the reduction reaction of cerium ion. The scandium ion favors the reduction extent by decreasing the lattice strain. However, when introducing up to 7%  $Sc^{3+}$ , the  $O_2$  production

decreases due to a decrease of the Ce content [53].  $\text{Ce}_{0.9}\text{Sc}_{0.1}\text{O}_2$  shows a higher amount of  $\text{O}_2$  released (2.21 mL/g) at 1500 °C compared to pure ceria (1.77 mL/g). Moreover, the  $\text{H}_2$  production and the re-oxidation yield are also increased compared to pure ceria, from 1.77 to 4.06 mL/g with 10% of Sc [53]. The Sc-doped ceria presents a rapid oxidation rate similar to pure ceria, although the addition of a dopant in ceria generally decreases the oxidation rate compared to pure ceria [58]. The average  $\text{H}_2$  production rate increased in presence of Sc ( $4.2 \text{ mL g}^{-1} \text{ min}^{-1}$ ) compared to pure ceria ( $1.9 \text{ mL g}^{-1} \text{ min}^{-1}$ ) [59]. Ceria doped with 10% of Sc provides a good production stability over cycles (for instance,  $\text{H}_2$  production of 4.04 mL/g during the 2<sup>nd</sup> cycle versus 3.92 mL/g during the 9<sup>th</sup> cycle) [53]. However, Scheffe et al. [58] found that Ce substitution by Sc does not enhance significantly the thermochemical performance.

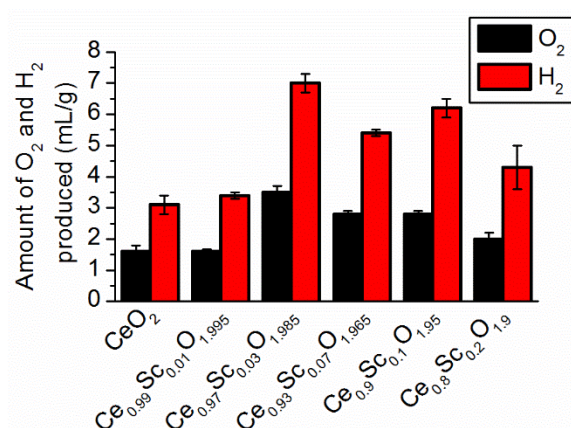


**Figure 4.** Amounts of  $\text{O}_2$  and  $\text{H}_2$  produced by Sc-doped ceria and pure ceria, with a reduction and oxidation temperature of 1500 °C and 500 °C, respectively [59].

Several studies reported a negative effect for the substitution of cerium by yttrium cation on thermochemical performance [55,60,61]. Jiang et al. [60] reported lower  $\text{O}_2$  production with yttrium insertion into ceria. Even if the oxygen vacancies formed during the reduction were more abundant than for pure ceria, their amount involved in the redox reaction was lower [60], thus yielding lower CO production [60,61]. Furthermore, the energy of O-vacancy formation was too low to drive the water-splitting reaction [56]. Similarly, Scheffe and Steinfeld [55] reported that the efficiency decreases with the increase of yttrium concentration.

Cobalt was also studied as a doping element for ceria. Ceria doped with 30% Co shows an oxygen production ( $9.4 \text{ Ncm}^3/\text{g}$ ) higher than pure ceria ( $4.8 \text{ Ncm}^3/\text{g}$ ) during the first cycle at 1500 °C. Co-doped ceria features maximum oxygen evolution rate, 3.6 to 5 times higher than for ceria. Nevertheless, the  $\text{O}_2$  production significantly decreases after the second cycle ( $2.9 \text{ Ncm}^3/\text{g}$ ) denoting a low material stability. Gokon et al. [62] highlighted that decreasing the reduction temperature did not increase the reduction duration, but it only decreased the maximum rate of oxygen evolution and the amount of produced oxygen. Furthermore, the  $\text{H}_2$  production was lower for Co-doped ceria ( $6.1 \text{ Ncm}^3/\text{g}$ ) than for undoped ceria ( $8.7 \text{ Ncm}^3/\text{g}$ ) with an oxidation temperature of 1150 °C [62]. The decrease of the ceria reduction temperature due to the incorporation of Co is interesting but the low thermal stability of Co-doped ceria may hinder large-scale application.

Jiang et al. [60] reported a negative effect of samarium addition into ceria on the O<sub>2</sub> production, with the same mechanism than for yttrium addition. The H<sub>2</sub> production is not increased by the samarium cation addition (108.6 μmol/g for Ce<sub>0.9</sub>Sm<sub>0.1</sub>O<sub>2</sub>) compared with pure ceria (125 μmol/g) at 1200 °C [63]. Scheffe and Steinfeld [55] proved that the increase in Sm concentration into ceria leads to a decrease of the solar-to-fuel energy conversion efficiency [55]. On the contrary, Bhosale and Takalkar [64] reported an increase of the reduction extent with the incorporation of 10% of Sm<sup>3+</sup> into CeO<sub>2</sub>. As an example, Ce<sub>0.9</sub>Sm<sub>0.1</sub>O<sub>2</sub> produces 173.3 μmol/g of O<sub>2</sub> against 53.3 μmol/g for CeO<sub>2</sub> at 1400 °C. However, the authors also showed that Sm-doped ceria led to slightly lower fuel production compared to pristine ceria (CO production of 108.1 μmol/g for Ce<sub>0.9</sub>Sm<sub>0.1</sub>O<sub>2</sub> and 110.4 μmol/g for CeO<sub>2</sub> at 1000 °C) [64].

Jiang et al. [60] and Ramos-Fernandez et al. [61] found that the use of lanthanum as ceria dopant does not improve the thermochemical performance. The CO generation rate did not increase and the produced amount was similar to that obtained with pure ceria [60,61]. Similarly, H<sub>2</sub> production did not increase by the incorporation of lanthanum (117.0 μmol/g) compared with pure ceria (125.0 μmol/g) at 1200 °C [63]. In contrast, Bhosale and Takalkar [64] highlighted a beneficial effect of the incorporation of La into CeO<sub>2</sub>. They reported an increase of the O<sub>2</sub> and CO production (161.8 μmol/g and 122.4 μmol/g, respectively) compared with pure ceria (53.3 μmol/g and 110.4 μmol/g, respectively) at reduction and oxidation temperatures of 1400 °C and 1000 °C, respectively. Nevertheless the average amount of CO produced by Ce<sub>0.9</sub>La<sub>0.1</sub>O<sub>2</sub> during nine consecutive cycles (98.0 μmol/g) is similar with pure ceria (94.9 μmol/g) [64].

The incorporation of 10% of Pr into CeO<sub>2</sub> was reported to decrease both O<sub>2</sub> and CO in comparison with pure ceria [64]. On the contrary, Meng et al. [65] showed that the reduction extent increased with a Pr concentration up to 10%. The Pr incorporation increases the quantity of available oxygen vacancies from the bulk to surface, leading to an improved O<sub>2</sub> release. Furthermore, the addition of Pr leads to an increase of the optimum oxidation temperature from 500 to 750 °C [65]. The oxidation state of Pr evolves from +IV to +III after the thermochemical cycle [66]. In porous structure with macro-interconnected porosities, the incorporation of Pr into CeO<sub>2</sub> causes a decrease of the open porosity in the range of 26–39% [67].

The effect of gadolinium incorporation in ceria revealed that H<sub>2</sub> production was not increased by the Gd cation (101.6 μmol/g for Ce<sub>0.9</sub>Gd<sub>0.1</sub>O<sub>2</sub>) compared with pure ceria (125 μmol/g) at 1200 °C [63]. In addition, Bhosale and Takalkar [64] reported that the incorporation of 10% Gd in ceria decreased both O<sub>2</sub> and CO productions in comparison with pure ceria.

The CeO<sub>2</sub> doping with 10% Tb<sup>3+</sup> permits to increase O<sub>2</sub> and CO production during the first cycle compared with pure CeO<sub>2</sub> [64]. However, the average amount of CO produced (80 μmol/g) during nine cycles is lower than the one for ceria (94.9 μmol/g), denoting a weak re-oxidation yield. The oxidation state of Tb evolves from +IV to +III after the thermochemical cycle [66]. The insertion of Er<sup>3+</sup> cation in place of Ce<sup>4+</sup> increases O<sub>2</sub> production, although CO production is lower than with pristine ceria. After 10 cycles, the Ce<sub>0.9</sub>Er<sub>0.1</sub>O<sub>2</sub> oxide displays higher increase of crystallite sizes compared to undoped ceria, revealing that the dopant does not enhance the thermal stability [64]. Ceria doped with Nd<sup>3+</sup> cation showed a decrease in both O<sub>2</sub> and CO productions in comparison with pristine ceria. However, the dopant improved the material stability [64]. Dy<sup>3+</sup> cation as ceria dopant had a negative effect on the amount of O<sub>2</sub> released according to Meng et al. [53]. In contrast, Bhosale

and Takalkar [64] observed quite similar O<sub>2</sub> production for both Ce<sub>0.9</sub>Dy<sub>0.1</sub>O<sub>2</sub> (53.2 μmol/g) and pure ceria (47.7 μmol/g) averaged over 9 cycles. Nevertheless, they reported lower CO production for Dy-doped ceria (87.3 μmol/g) compared to pristine ceria (94.9 μmol/g) averaged over 9 cycles. The increasing rate of crystallite sizes was limited by the presence of Dy dopant into ceria, suggesting an improved thermal stability [53].

Muhich and Steinfeld [56] stated that divalent and trivalent elements were not suitable dopants. Indeed, two electrons must be promoted to the Ce f-band upon reduction if the energy required to drive water splitting is not sufficient. Divalent and trivalent elements did not promote two electrons to the Ce f-band. The authors rather suggested to use tetravalent dopants to improve significantly the thermochemical performance of ceria [56]. Among the trivalent dopants presented previously, only Sc showed a significant improvement of the thermochemical performance of ceria. Other dopants did not present any meaningful increase of the fuel production or improvement of the thermal stability.

### 3.4. Tetravalent dopants

The use of tetravalent cations with ionic radius smaller than Ce<sup>4+</sup>, as ceria dopants, can increase ceria thermochemical performance. Their small ionic radius permits to decrease the oxygen diffusion barrier and facilitates vacancy formation, thus enhancing O<sub>2</sub> production. The onset reduction temperature is lowered for ceria doped with tetravalent cation compared with pure ceria [29,60]. The incorporation of tetravalent cations into ceria favors the formation of active oxygen vacancies and decreases the energy of vacancy formation [29,66].

The ceria–zirconia solid solution is composed of tetragonal or monoclinic phase. At high ceria content ( $x \leq 0.15$ ), Ce<sub>1-x</sub>Zr<sub>x</sub>O<sub>2</sub> has a fluorite structure. Three tetragonal phases (t, t', t'') are reported for  $0.15 \leq x \leq 0.85$  [68]. When focusing on redox-active materials, the Zr-concentration in ceria-zirconia is generally limited to 50%, and beyond there is no beneficial effect on the thermochemical performance. The phase diagram can be found elsewhere [69]. The presence of pyrochlore structure (Ce<sub>2</sub>Zr<sub>2</sub>O<sub>7</sub>) has also been reported [70]. It consists of an ordered structure where 1/8 of the anion is missing. This phase has a beneficial effect on the reduction extent [71]. However, no study has demonstrated the beneficial effect for fuel production. The reduction extent of Zr-doped ceria is enhanced with the increase of Zr concentration (Figure 5) [58,72–75]. The 10% Zr-doped ceria presents a lower onset temperature (~750 °C) compared to pure ceria (1000 °C) [58,76]. The reduction temperature can thus be decreased below 1500 °C by Zr incorporation [72,77]. The enhancement of the reduction step is due to an improved oxygen mobility caused by lattice distortion and the favored oxygen vacancies due to the incorporation of the Zr dopant [77,78]. The Zr–O bonds are tensilely strained and in this way they store energy, that is released with oxygen vacancy formation during the reduction step. The release of oxygen is then promoted with the presence of zirconium dopant [56]. The oxygen anions (still four-coordinated) next to the doping center show considerably lower reduction energies (by 0.6 eV) and larger displacements. An O vacancy is more easily created close to the Zr centers, therefore they might serve as nucleation centers for vacancy clustering. The electrons remaining after the oxygen release are localized on two Ce cations neighboring the vacancy, which results in the reduction of two Ce<sup>4+</sup> ions [79]. The reducible cation is Ce and an oxygen vacancy has two associated Ce(III) as proved by scanning tunneling

microscopy [80]. The oxygen vacancies can be single, double, multiple, located at either the surface or the subsurface. From a thermodynamic point of view, the incorporation of Zr into ceria leads to a decrease of the partial molar enthalpy compared with pure ceria [74]. The reduction of ceria-zirconia can be considered as a removal of oxygen on the basis of “pyrochlore-like” structures (reduction of  $\text{Ce}_2\text{Zr}_2\text{O}_8$  to  $\text{Ce}_2\text{Zr}_2\text{O}_7$ ) depending on the number of sites from which oxygen can be removed. The “pyrochlore-like structure” can thus help to explain the enhanced redox properties of ceria-zirconia [81]. Ceria doped with 10% Zr has a faster oxygen production rate than pure ceria due to a lower activation energy (162 kJ/mol) in comparison with pure ceria (235 kJ/mol) [61]. Jiang et al. [60] evidenced that  $\text{Zr}^{4+}$  doped ceria shows the highest  $\text{O}_2$  production compared to ceria doped with other tetravalent ions ( $\text{Ti}^{4+}$ ,  $\text{Sn}^{4+}$ ,  $\text{Hf}^{4+}$ ). In contrast, Muhich et al. [82] predicted a lower reduction capability for Zr– $\text{CeO}_2$  in comparison with Hf– $\text{CeO}_2$  [82]. Indeed, the addition of Zr in ceria promotes bulk reduction at lower temperature than for undoped ceria [75].

Conversely, the incorporation of Zr may have a negative effect on the oxidation step. The required oxidation temperature is generally lowered, thus leading to higher temperature swing [74,83], while the oxidant gas has to be supplied in excess [84] when compared with pure ceria. The slow oxidation of Zr-doped ceria is explained by a thermodynamically less favorable reaction than for pristine ceria [74] because of decreasing Ce(III) ions concentration at the ceramic surface induced by Zr dopant [58,61,75]. The CO production with  $\text{Ce}_{0.75}\text{Zr}_{0.25}\text{O}_2$  was found to be higher than for undoped ceria at an oxidation temperature of 1200 °C and 1300 °C. However, for an oxidation temperature of 1400 °C, undoped ceria shows higher CO production than  $\text{Ce}_{0.75}\text{Zr}_{0.25}\text{O}_2$  [60]. The activation energy of the  $\text{CO}_2$  splitting reaction is in the range 83–103 kJ/mol for  $\text{Zr}_{0.25}\text{Ce}_{0.75}\text{O}_2$ , depending on the synthesis route. Furthermore, the oxidation step is best described by a diffusion model, meaning that bulk reduction associated with powder sintering prevails and the reaction is controlled by a diffusion-limited regime. The Zr-doped ceria may also show reactivity decrease over cycles due to its lower thermal resistance than pure ceria [85]. Concerning the hydrolysis reaction, the activation energy was calculated to be 51 kJ/mol for  $\text{Ce}_{0.75}\text{Zr}_{0.25}\text{O}_2$  [77].

A few studies [83,84,86] have evaluated the solar-to-fuel energy conversion efficiency of Zr-doped ceria using thermodynamic analysis. It was shown that Zr-doped ceria materials offer higher efficiency than pure ceria in most conditions [83,84,86]. Ganzoury et al. [84] demonstrated that, under isothermal conditions (at 1800 °C) with a gas heat recovery of 90%,  $\text{Ce}_{0.95}\text{Zr}_{0.05}\text{O}_2$  has an efficiency of 0.032% (versus 0.005% for pure ceria). For an oxidation temperature in the range 600–900 °C, Zr-doping has a negative impact on ceria efficiency. An increase or decrease of the oxidation temperature out from this range results in an improvement of the solar-to-fuel energy conversion efficiency [84]. Bulfin et al. [83] also suggested the importance of lowering the oxidation temperature (<800 °C) compared with pure ceria, to improve the efficiency of Zr-doped ceria [83]. Muhich et al. [86] carried out a thermodynamic analysis for assessing the solar-to-fuel energy conversion efficiency for different non-stoichiometric oxides. The authors showed that Zr-doped  $\text{CeO}_2$  yielded the highest efficiency whatever the operating conditions, except the case of  $\text{CO}_2$  splitting with high solid heat recovery for which pure ceria remains the most efficient material [86].

Zr-doped ceria shows a higher maximum non-stoichiometry than pristine ceria. However, the oxidation kinetics are slower than for undoped ceria. To overcome this issue, a number of studies investigated the incorporation of a second dopant. Call et al. [87] used lower valence cations in

$\text{Ce}_{0.85}\text{Zr}_{0.15}\text{O}_2$ , but they concluded that this route was not beneficial for enhancing  $\text{O}_2$  and CO production. The incorporation of bigger trivalent ions leads to an increase of the lattice strain, which decreases the amount of produced oxygen, compared to  $\text{Ce}_{1-x}\text{Zr}_x\text{O}_2$ . However,  $\text{Ce}_{1-x}\text{Zr}_x\text{O}_2$  doped with lower valence cation can reduce the reactivity decrease of  $\text{Ce}_{1-x}\text{Zr}_x\text{O}_2$  upon cycling [87].

Le Gal et al. [75] investigated the impact of the incorporation of trivalent lanthanides (Y, La, Pr and Gd) in Zr-doped ceria. They highlighted that Y, La and Pr dopants did not provide any improvement on the oxide reducibility, although they had a beneficial impact on its thermal stability. The kinetic limitation observed during the second oxidation step for Zr-doped ceria decreases thanks to the incorporation of these dopants [75]. However, in other studies, the incorporation of 1% of Gd ( $\text{Ce}_{0.74}\text{Zr}_{0.25}\text{Gd}_{0.01}\text{O}_2$ ) improved the oxide reduction extent (200  $\mu\text{mol/g}$  of  $\text{O}_2$  produced at 1400 °C) when compared with pure ceria and 25% Zr-doped ceria (75.0  $\mu\text{mol/g}$  and 179.4  $\mu\text{mol/g}$ , respectively). Moreover, during the oxidation step the  $\text{H}_2$  produced with  $\text{Ce}_{0.74}\text{Zr}_{0.25}\text{Gd}_{0.01}\text{O}_2$  (338  $\mu\text{mol/g}$ ) is higher than for both  $\text{CeO}_2$  and  $\text{Ce}_{0.75}\text{Zr}_{0.25}\text{O}_2$  (128.0  $\mu\text{mol/g}$  and 323.0  $\mu\text{mol/g}$ , respectively). The crystallite growth was hindered due to the presence of Gd and the performance was reported to decrease for higher Gd concentration [63]. On the contrary, Call et al. [87] reported that the incorporation of Gd dopant into  $\text{Ce}_{0.85}\text{Zr}_{0.15}\text{O}_2$  results in lower  $\text{O}_2$  and CO production in comparison with pristine  $\text{Ce}_{0.85}\text{Zr}_{0.15}\text{O}_2$ .

Kang et al. [88] investigated the effect of Ni, Fe, Mn and Mg as dopants in ceria-zirconia. They reported that these dopants increase the  $\text{O}_2$  production during the first cycle compared with ceria-zirconia. Nevertheless,  $\text{Ce}_{1-x}\text{Zr}_x\text{O}_2$  doped with Ni, Fe, and Mn shows a weak CO/ $\text{O}_2$  ratio (e.g., 0.35 for  $\text{Ce}_{0.7}\text{Zr}_{0.2}\text{Mn}_{0.1}\text{O}_2$ ). Only the Mg dopant presents a good CO/ $\text{O}_2$  ratio (1.52 and 1.99 for the first and second cycles, respectively). The CO production increases from 4.65 to 5.64 mL/g with 10% addition of Mg in  $\text{Ce}_{0.8}\text{Zr}_{0.2}\text{O}_2$  [88]. The introduction of Mg in Zr-doped ceria engenders lattice defects in the crystalline structure, which increases oxygen mobility. The thermal stability is also improved by the incorporation of Mg. Calcium dopant was also identified by Kang et al. [89] to be beneficial for both the oxygen mobility and the thermal stability of Zr-doped ceria [89].

The samarium cation was suggested as an efficient dopant to prevent the decrease of oxidation kinetics due to its sintering effect in Zr-doped ceria. However, fuel production with Sm-doped ceria-zirconia is lower than with the pristine Zr-doped ceria. The initial strain in the crystal lattice due to the oxygen vacancy formation is increased with the incorporation of  $\text{Sm}^{3+}$  into Zr-doped ceria, owing to the bigger ionic radius of  $\text{Sm}^{3+}$  compared to  $\text{Ce}^{4+}$ . The zirconium cation cannot compensate this expansion, leading to a lower amount of oxygen released. However,  $\text{Ce}_{0.82}\text{Zr}_{0.15}\text{Sm}_{0.03}\text{O}_2$  provides a stable fuel production yield contrary to Zr-doped ceria. After 100 cycles, Zr-doped ceria undergoes a 30% decrease of its CO production, whereas  $\text{Ce}_{0.82}\text{Zr}_{0.15}\text{Sm}_{0.03}\text{O}_2$  shows a negligible decrease of the produced CO amount [87]. The addition of samarium into Zr-doped ceria does not improve the oxygen and fuel production, but increases thermal stability [63,87].

The addition of  $\text{Hf}^{4+}$  in Zr-doped ceria has also been investigated. Among the tested formulations,  $\text{Ce}_{0.895}\text{Zr}_{0.046}\text{Hf}_{0.053}\text{O}_{1.988}$  provides the highest performance in comparison with undoped ceria-zirconia. The Hf-doped material successfully underwent 20 thermochemical cycles with average productions of 114  $\mu\text{mol/g}$  of  $\text{O}_2$  (1400 °C) and 162  $\mu\text{mol/g}$  of CO (1000 °C). A grain growth was observed during the first cycle due to sintering, but then no further grain growth occurred during the 19 following cycles [90].

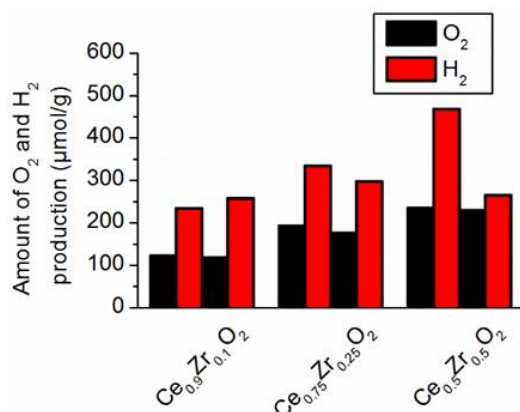


**Figure 5.** O<sub>2</sub> and H<sub>2</sub> production during two thermochemical cycles using Ce<sub>1-x</sub>Zr<sub>x</sub>O<sub>2</sub> (x = 0.1, 0.25 and 0.5) with reduction and oxidation temperatures of 1400 °C and 1050 °C, respectively [77].

The dopant radius has an influence on the thermochemical properties. The radius able to give the best performance was calculated by Jacot et al. [66] to be around 0.8 Å. The Hf<sup>4+</sup> cation (8-fold coordination) has a ionic radius of 0.83 Å, and should thus provide attractive thermochemical performance [66]. The reduction extent of Hf-doped ceria increases with Hf dopant concentration [58]. For example, Meng et al. [53] observed an increase of 67% in O<sub>2</sub> production when adding 10% Hf, in comparison with undoped ceria [53]. The addition of Hf<sup>4+</sup> cation permits to compensate the ceria lattice expansion during the reduction step by storing the energy in tensile strained Hf–O bond. This contributes to increase the oxygen release [56]. The 10% Hf-doped ceria presents a lower onset temperature (~750 °C) than pure ceria (1000 °C) [58]. The onset reduction temperature increases with the Hf concentration, reaching 930 °C for Ce<sub>0.8</sub>Hf<sub>0.2</sub>O<sub>2</sub>. At the same time, the increase of Hf concentration leads to an increase of the time required to fully oxidize the doped ceria. This trend is illustrated in Figure 6 [67]. The oxidation kinetics for Ce<sub>0.93</sub>Hf<sub>0.07</sub>O<sub>2</sub> were observed to be slower than for undoped ceria [66]. H<sub>2</sub> production is increased by the larger non-stoichiometry reached during the reduction step compared with pure ceria. However, the re-oxidation yield of Hf-doped ceria is lower than for undoped ceria [53]. A decrease of the produced H<sub>2</sub>:O<sub>2</sub> ratio is observed for Ce<sub>0.9</sub>Hf<sub>0.1</sub>O<sub>2</sub> over cycles (1.76 for the 2<sup>nd</sup> cycle down to 1.47 for the 9<sup>th</sup> cycle) [53]. Scheffe et al. [58] showed that fuel production was more influenced by the kinetic rate than by thermodynamic limitations. The maximum H<sub>2</sub> production was obtained with Hf concentration of 10%. After three cycles, a decrease of both the specific surface area (from 1.41 to 0.66 m<sup>2</sup>/g) and the oxidation rate was noticed. The decrease of the former cannot be clearly related to the low oxidation rate since pure ceria also presents a similar decrease of specific surface area (from 1.37 to 0.39 m<sup>2</sup>/g) but without any decrease of the oxidation rate [58]. Jiang et al. [60] reported a phase separation after high-temperature reactions for Hf dopant concentration beyond 25% [60].

The incorporation of lower valence dopants (Li<sup>+</sup>, Mg<sup>2+</sup>, Ca<sup>2+</sup>, Er<sup>3+</sup> and Y<sup>3+</sup>) into Ce<sub>0.95</sub>Hf<sub>0.05</sub>O<sub>2</sub> was investigated by Jacot et al. [91] aiming to improve the redox reaction kinetics. For all the investigated dopants, the reduction kinetic was not improved whereas the oxidation kinetic enhancement was weak [91]. However, the addition of Li<sup>+</sup> dopant into Hf-doped CeO<sub>2</sub> helps to

preserve the interconnected porosity compared with undoped ceria. The lithium reduces the cation mobility at high temperature, thus maintaining the interconnected porosity [67].

Meng and Tamaura [92] studied the addition of Pr into Hf-doped ceria. The X-ray diffraction analysis showed that the Pr cation is present in the solid solution as tetravalent and trivalent states. The introduction of 10% Pr into  $\text{Ce}_{0.9}\text{Hf}_{0.1}\text{O}_2$  increased the  $\text{H}_2$  production (5.72 mL/g) in comparison with the pristine  $\text{Ce}_{0.9}\text{Hf}_{0.1}\text{O}_2$  (4.50 mL/g). The multivalent states of Pr cation led to the enhancement of thermochemical properties by eliminating residual gaseous oxygen ( $\text{Pr}^{3+}$  oxidation into  $\text{Pr}^{4+}$ ) and improving the ionic conductivity of the oxide [92].

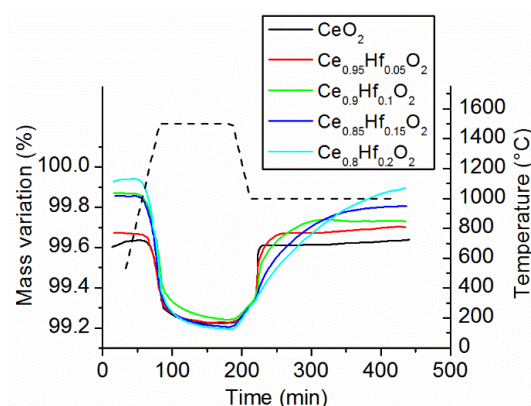
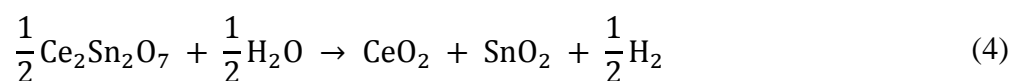
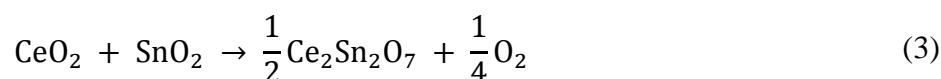


**Figure 6.** Thermogravimetric analysis of  $\text{Ce}_{1-x}\text{Hf}_x\text{O}_2$  during a reduction at 1500 °C followed by an oxidation under  $\text{CO}_2$  at 1000 °C [67].

The presence of titanium into ceria enhances the  $\text{O}_2$  production compared with pure ceria, although a new phase of  $\text{Ce}_2\text{Ti}_2\text{O}_7$  was formed after thermochemical cycling [60,66], leading to lower amounts of produced CO [60,61]. The energy of vacancy formation decreased thanks to the presence of titanium cation because only three oxygen bonds need to be broken to release oxygen due to the smaller ionic radius of titanium compared to cerium. However, Ti cations tend to attract each other and form Ti cations pairs which vacancy formation energy is too low to drive the water splitting reaction [56].

Jiang et al. [60] investigated the use of Sn as ceria dopant. The presence of 20% of Sn in ceria increased the reduction extent by five times compared to pure ceria [60]. This was due to a low energy of vacancy formation [29]. However, a  $\text{Ce}_2\text{Sn}_2\text{O}_7$  phase was formed during reduction of ceria doped with 20% Sn, which leads to low amount of produced CO during the oxidation step [60]. Besides, Ruan et al. [93] investigated the  $\text{CeO}_{2-x}\text{SnO}_2/\text{Ce}_2\text{Sn}_2\text{O}_7$  pyrochlore cycle as follows:



During the reduction (Eq 3), the  $\text{Ce}_2\text{Sn}_2\text{O}_7$  pyrochlore is formed from  $\text{CeO}_2$  and  $\text{SnO}_2$ . During the following re-oxidation step (Eq 4),  $\text{Ce}_2\text{Sn}_2\text{O}_7$  is re-oxidized by water and  $\text{CeO}_2$  and  $\text{SnO}_2$  are regenerated. The authors reported 4.87 mL/g of  $\text{O}_2$  with  $\text{CeO}_2\text{-}0.15\text{SnO}_2$ , while only 1.03 mL/g was obtained with pure ceria at 1400 °C. The  $\text{H}_2$  production is higher with  $\text{CeO}_2\text{-}0.15\text{SnO}_2$  (7.18 mL/g) than with pristine ceria (1.87 mL/g), even if the oxidation rate is slower for the former material. Seven consecutive cycles have been performed with  $\text{CeO}_2\text{-}0.15\text{SnO}_2$  without decrease of the fuel production, thus showing a good stability of the material [93].

The tungsten cation used as dopant into ceria does not provide any significant enhancement of thermochemical performance compared with pure ceria [61]. Rhodium has been studied as ceria dopant by Lin et al. [94] who reported that this dopant increased the formation of oxygen vacancies in ceria [94]. However, Jacot et al. [66] reported that  $\text{Ce}_{0.9}\text{Rh}_{0.2}\text{O}_2$  suffers from important and irreversible mass loss during thermogravimetric analysis, thus altering the re-oxidation step [66]. Furthermore, rhodium is one of the rarest and most valuable precious metals and its use may thus be not favorable for process economics.

The addition of Si and Ge into ceria has been studied by Andersson et al. [29]. In both cases, a higher reduction extent was obtained in comparison with pure ceria. These dopants favor the formation of a tetrahedral arrangement in the surrounding of  $4^+$  cations leading to strongly distorted lattice structure. Most of the oxygen release is due to lattice relaxation caused by the formation of oxygen vacancies [29]. The ceria doped with 10% Si shows however an irreversible mass loss during thermogravimetric analysis, impeding further water or  $\text{CO}_2$  splitting [66].

The addition of chromium into ceria has been attempted to improve ceria thermochemical performance. Cr was identified in ceria, either as a dopant and/or as chromic clusters. The  $\text{CeCrO}_3$  perovskite phase formed during the reduction step contributes to increase the amount of  $\text{O}_2$  released, although this perovskite phase does not participate in the redox cycle [66,95]. When a chromic phase is present on the oxide surface, it improves the oxidation step. Indeed, the oxygen uptake is increased by chromium as well as the oxidation kinetics [95]. During the redox cycle, Cr(III) converts to Cr(IV) revealing an unstable oxidation state [66]. In contrast, Ramos-Fernandez et al. [61] found that the use of chromium as ceria dopant does not improve the thermochemical performance. The CO generation rate was not increased and the amount of fuel produced was similar to pure ceria [60]. The use of chromium may not be advised, as it can be dangerous for health and environment.

### 3.5. Pentavalent dopants

The incorporation of  $\text{Nb}^{5+}$  cation into ceria contributes to increase the reduction extent in comparison with pure ceria [66,91]. The highest  $\text{O}_2$  amount released was reached with 5% Nb-dopant concentration. This formulation displays a slightly higher non-stoichiometry ( $\delta = 0.034$ ) in comparison with pure ceria ( $\delta = 0.029$ ) [91]. Jacot et al. [66] reported that before cycling, ceria doped with 10% Nb contain a secondary phase  $\text{Ce}_3\text{NbO}_7$ , which transforms to  $\text{CeNbO}_4$  after the redox cycle [66]. The small ionic radius of Nb and its strong covalent characteristic results in a decrease of the vacancy formation energy because only three oxygen bonds have to be broken during the reduction. However, the Nb dopant might also form clusters. In this configuration, only the oxygen vacancies situated far from the Nb dopant are able to drive water-splitting, thus leading to

weak H<sub>2</sub> production [56]. Furthermore, Nb may be toxic, limiting its application in future industrial processes.

Hoes et al. [96] investigated the introduction of a second dopant (La, Y, Sc) in Nb-doped ceria. They showed that the reduction extent achieved by these oxides decreases in the following order: Ce<sub>0.9</sub>Sc<sub>0.05</sub>Nb<sub>0.05</sub>O<sub>2</sub> > Ce<sub>0.9</sub>Y<sub>0.05</sub>Nb<sub>0.05</sub>O<sub>2</sub> > Ce<sub>0.95</sub>La<sub>0.025</sub>Nb<sub>0.025</sub>O<sub>2</sub> > Ce<sub>0.75</sub>La<sub>0.125</sub>Nb<sub>0.125</sub>O<sub>2</sub> > CeO<sub>2</sub>. The highest calculated energy efficiency was achieved by Ce<sub>0.9</sub>Y<sub>0.05</sub>Nb<sub>0.05</sub>O<sub>2</sub> (31% with H<sub>2</sub>O vapor as oxidant) in comparison with 26% for pure ceria [96].

The use of tantalum cation as dopant into CeO<sub>2</sub> increases the reduction extent [63,66,91]. The highest reduction extent was reached with 7% Ta-dopant concentration [91]. Doping ceria with 10% Ta increases the H<sub>2</sub> production compared with undoped ceria (142 μmol/g of H<sub>2</sub> produced at 1040 °C after a reduction at 1450 °C). However, Jacot et al. [66] noticed that the re-oxidation kinetics of Ce<sub>0.93</sub>Ta<sub>0.07</sub>O<sub>2</sub> was slower compared to pure ceria [66]. The formation of a stable CeTaO<sub>4</sub> phase was observed for Ta-dopant concentration of 25% and 50% during the reduction step [63]. Jacot et al. [66,91] reported the presence of CeTa<sub>3</sub>O<sub>9</sub> phase in the as-synthesized 7% Ta-doped ceria [66,91]. Upon cycling, Ta-doped ceria presents a decrease of the weight loss during O<sub>2</sub> release (0.580% to 0.470%), which may be attributed to the formation of Ce-rich phases prone to evaporate [91]. Muhich and Steinfeld [56] predicted that the addition of Ta into ceria does not enhance its thermochemical performance [56].

Likewise, the use of vanadium as ceria dopant does not improve the ceria redox activity [56]. This was confirmed by Jacot et al. [66], who noticed the presence of a CeVO<sub>4</sub> phase after the synthesis of Ce<sub>0.9</sub>V<sub>0.1</sub>O<sub>2</sub>. Moreover, the thermochemical performance of this formulation does not provide any improvement in comparison with pristine ceria [66].

### 3.6. Dopants with multiple oxidation states

Manganese has been studied as ceria dopant: during the first cycle, ceria doped with 30% Mn showed an improved O<sub>2</sub> production (13.2 Ncm<sup>3</sup>/g) compared with pure ceria (4.8 Ncm<sup>3</sup>/g) at a reduction temperature of 1500 °C. The maximum rate of oxygen evolution achieved by Mn-doped ceria was 8.1 to 9.5 times higher than for ceria. However, during the second cycle the O<sub>2</sub> production of Mn-doped ceria fell down to 5.4 Ncm<sup>3</sup>/g, i.e., similar to pure ceria. In addition, the H<sub>2</sub> amount produced was smaller with Mn-doped ceria (7.9 Ncm<sup>3</sup>/g) than with undoped ceria (8.7 Ncm<sup>3</sup>/g) at 1150 °C [62].

Iron was another investigated dopant: ceria doped with 30% Fe presents a high O<sub>2</sub> production (10.5 Ncm<sup>3</sup>/g) compared with pure ceria (4.8 Ncm<sup>3</sup>/g) at 1500 °C. However, the material melted at this temperature [62]. The presence of Fe<sup>2+</sup> and Fe<sup>3+</sup> in the crystal lattice increases the oxygen mobility, thus leading to enhanced O<sub>2</sub> and H<sub>2</sub> productions. However, both O<sub>2</sub> and H<sub>2</sub> productions were not influenced by the Ce:Fe ratio [31].

Ceria doped with 30% Ni shows a weak enhancement of O<sub>2</sub> and H<sub>2</sub> productions (4.4 Ncm<sup>3</sup>/g and 9.0 Ncm<sup>3</sup>/g, respectively) compared with pure ceria (4.8 Ncm<sup>3</sup>/g and 8.7 Ncm<sup>3</sup>/g, respectively) at temperatures of 1500 °C and 1150 °C, respectively [62]. Kaneko and Tamaura [97] highlighted the highest O<sub>2</sub> and H<sub>2</sub> amounts obtained (1.4 Ncm<sup>3</sup>/g and 2.5 Ncm<sup>3</sup>/g, respectively) with a molar Ce:Ni

ratio of 9.5:0.5. The Ni cation is involved in the formation of anionic defects that promote the oxygen mobility [97].

The addition of Zn into ceria was also investigated. A significant amount of ZnO was detected in the fresh sample, but after few cycles, the ZnO phase sublimated (traces of ZnO were still present afterwards) while Zn was still present as dopant in the ceria solid solution. The ZnO phase had an adverse effect on the H<sub>2</sub> and CO productions. However, the Zn dopant contributed to increase the ceria redox activity. Furthermore, Zn-doped ceria showed a stable fuel production over consecutive cycles [98].

### 3.7. Paired charge compensating strategy

Muhich et al. [82] investigated a doping strategy of ceria using paired charge compensating dopants. Ceria was co-doped with a trivalent cation (Sc, Y, or La) and a pentavalent cation (V, Nb or Ta). The trivalent dopant has an important impact on the reduction step, caused by the decrease of the ionic attraction between trivalent cation and oxygen anion in comparison with Ce<sup>4+</sup> and O<sup>2-</sup>. Inversely, the pentavalent cation has only a small effect on the reduction step. Among the compositions investigated, Ce<sub>0.9</sub>Sc<sub>0.05</sub>X<sub>0.05</sub>O<sub>2</sub> (with X = V, Nb or Ta) exhibits the highest reduction capability. However, it still remains lower than Hf-doped ceria [82].

The thermochemical performance of ceria needs to be improved in order to reach an economically viable solar fuel production. However, modifying ceria properties using dopants is complex, as dopants influence more than one property. None of the dopants presented so far allows a significant improvement of ceria performance. However, some of them appear promising, especially zirconium that increases the reduction extent at the expense of a decrease of the oxidation rate and thermal stability. Scandium may also be attractive since it increases O<sub>2</sub> production and promotes the thermal stability. Hafnium increases the reduction extent as well while decreasing the onset temperature. However, the re-oxidation yield decreases over cycles. Another important lever to improve thermochemical performance is the shaping of the reactive ceria-based materials for tailoring both their microstructure and morphology.

## 4. Material shape design

The solar-to-fuel energy conversion efficiency is not only influenced by the chemical composition of the reactive compound, but also by the material shaping that mostly determines the available surface area for the solid/gas reaction (the material oxidation mechanism is mainly governed by surface reaction). The diffusion length and specific surface area affect respectively the reduction and oxidation steps. They depend on the morphology of the reactive material. Accordingly, the main relevant options for materials shaping are summarized in this section.

### 4.1. Felts and fibers

Furler et al. [7] used porous CeO<sub>2</sub> felt to perform thermochemical cycles. Over ten cycles, 2.89 mL/g of O<sub>2</sub> and 5.88 mL/g of fuel were produced in average. Due to low heat absorption and the

presence of hot spots, ceria sublimates and forms an opaque film on the optical window, contributing to a decrease of temperature. The solar-to-fuel efficiency was 0.09% for ten consecutive cycles [7]. Such a low efficiency was attributed to the low thermal conductivity of the felt, leading to heat transfer limitations. Hence, the reaction is mainly limited to the near surface directly exposed to the concentrated sunlight [41,99].

Gibbons et al. [100] investigated electrospun ceria-based fibers in order to maintain both high surface area and small grain sizes. The fiber diameter is in the range 100 nm–2  $\mu\text{m}$ . The oxidation reaction kinetic was increased by the specific surface area of the fibers. The electrospun structure impedes the sintering responsible for the decreasing production of fuel over cycles. The specific surface area of  $\text{Ce}_{0.975}\text{Zr}_{0.025}\text{O}_2$  drops to 0.60  $\text{m}^2/\text{g}$  after a thermal reduction at 1400  $^\circ\text{C}$ . This is mainly due to an increase of grain sizes along the fiber axis. However, the decrease of specific surface area does not cause a decrease in CO production. During long-term cycling, the CO production rate declines from 30 after few cycles to 13–14  $\text{mL min}^{-1} \text{g}^{-1}$  after 60 cycles [100].

Gladden and Davidson [101] studied the use of ceria fibers made with a commercially suitable manufacturing process for the aim of producing fibers applicable to different reactor types. In isothermal conditions (1500  $^\circ\text{C}$ ), the microstructure was still open and porous with a porosity of 73% after 1000 cycles, although the specific surface area dropped from 0.143 to 0.078  $\text{m}^2/\text{g}$ . Regardless of the weak surface area, the fiber-mat design remained an appropriate strategy in isothermal conditions, as fuel production was governed by thermodynamics. In the case of temperature-swing redox cycling (from 800 to 1500  $^\circ\text{C}$ ), the specific surface area dropped to 0.057  $\text{m}^2/\text{g}$  after 1000 cycles. However, the open and porous structure of the fiber-mat was still retained [101].

#### 4.2. Reticulated porous foams

In order to avoid the inherent limitations induced by the use of a felt material, several studies focused on the application of reticulated porous foams [2,41,47,99,101–106]. The use of ceria-based reticulated porous ceramics (RPC) with a macroporous structure (mm-pore sized) improves the penetration and the volumetric absorption of incident concentrated solar radiation. In this way, the temperature gradient through the foam structure is lowered, thus promoting  $\text{O}_2$  production during homogeneous reduction of the whole loaded material [41]. The reduction duration of RPC ceria was predicted to be in the order of seconds, namely longer than with reactive particles due to the longer bulk diffusion lengths [50]. Furler et al. [102] obtained a solar-to-fuel energy conversion efficiency of about 1.73% (with 2.8–3.8 kW power input), almost 17 times higher than for ceria felt. However, the maximal fuel production rate is 9 times lower for a RPC foam than for a felt. The oxidation reaction is a surface-controlled reaction and the RPC structure has a low geometric specific surface area, yielding slow oxidation rates [102]. Takacs et al. [103] obtained the highest heat transfer with large pore sizes, i.e., foam with 8 pores per inch (ppi), although the highest  $\text{O}_2$  amount produced was obtained with a 10 ppi foam thanks to its higher pore density [103]. Cho et al. [104] developed a MgO partially-stabilized zirconia foam coated with reactive ceria to perform thermochemical cycles. Over seven cycles, the foam produced 4573 mL of  $\text{H}_2$  in total (for 82.88 g of loaded reactive ceria), with a reduction temperature in the range 1400–1600  $^\circ\text{C}$  and an oxidation temperature in the range 900–1100  $^\circ\text{C}$  [104].

Foams with only macropores feature good solar absorption properties, thus promoting the reduction step. However, the oxidation step is not favored due to the poor specific surface area of the reticulated foam. In order to improve the oxidation rate, dual-scale porosity RPC foams were developed by Furler et al. [47] with combined macro-scale (mm-pore sized) and micro-scale porosity ( $\mu\text{m}$ -pore sized). Firstly, millimetric pores permit volumetric absorption of concentrated sunlight and efficient heat transfer to the reactive material. Secondly, micrometric pores improve the specific surface area, which promotes the oxidation step by improving the reaction kinetics [2,47,105,106]. Furler et al. [47] obtained reduced cycling time and solar-to-fuel efficiency of 1.72% without sensible heat recovery [47]. Marxer et al. [106] carried out 291 cycles with stable redox performance, yielding the production of 700 NL of syngas. The reactive material undergoes sintering, resulting in an increase of grain size, but micro-scale pores still remain open. Dual-scale RPC provides faster oxidation rate ( $0.75 \text{ mL min}^{-1} \text{ g}^{-1}$ ) and higher fuel amount produced (4.41 mL/g) in comparison with single-scale RPC ( $0.37 \text{ mL min}^{-1} \text{ g}^{-1}$  and 4.11 mL/g, respectively). However, regarding the study of Marxer et al. [106], the mass loaded of dual-scale RPC in the reactor (948 g) is lower than the one of single-scale RPC (1413 g). This leads to an absolute amount of CO produced by dual scale RPC (4.18 L) lower than for single scale RPC (5.80 L) [106]. It should be noticed that the use of polymer templates to synthesize the reticulated porous foams is not environmentally friendly and should be replaced by bio-based templates for proposing sustainable processes.

#### 4.3. Nanostructured powders

Venstrom et al. [107,108] developed a nanocrystalline three-dimensionally ordered macroporous (3DOM) ceria powder. The powder has a surface area of  $29.9 \text{ m}^2/\text{g}$  before cycling with average grain sizes of 14 nm and an interconnected ordered porous network. The authors carried out the reduction at 1100 K under 5%  $\text{H}_2$  in Ar, followed by an isothermal oxidation with either  $\text{H}_2\text{O}$  or  $\text{CO}_2$  [107,108]. In comparison with commercial ceria powder, the  $\text{H}_2$  ( $\text{CO}$ ) production rate is 126% (260%) faster with 3DOM powder, as observed in Figure 7. This is due to the high specific surface area ( $10.2 \text{ m}^2/\text{g}$ ) of the 3DOM powder remaining after the reduction. The powder morphology clearly affects the oxidation kinetic. However, the amount of fuel produced is comparable between the 3DOM and the commercial powder ( $23 \text{ Ncm}^3/\text{g}$  of CO and  $20 \text{ Ncm}^3/\text{g}$  of  $\text{H}_2$ ). However, the ordered structure is not stable after 1h thermal treatment at  $1250 \text{ }^\circ\text{C}$ , but porosity is still present [107]. Costa Oliveira et al. [109] investigated 3DOM ceria particles prepared from cork template. The CO production of the 3DOM structure is twice higher than with reticulated porous ceria, proving that the 3DOM morphology enhances oxidation kinetic. Ceria granules were able to produce stable amount of CO over 11 solar-driven cycles and the ordered structure was retained after cycling. The CO peak production rate of 3DOM particles was three times higher than the value reported for dual-scale reticulated porous ceria [109].

Hierarchical pore structure of ceria was developed by Malonzo et al. [110] using wood template. The structure, consisting of micrometer-thick walls, pore size of  $10 \mu\text{m}$  and a specific surface area of  $0.1 \text{ m}^2/\text{g}$ , is retained after undergoing cycles up to  $1400 \text{ }^\circ\text{C}$ . For a reduction temperature of  $1500 \text{ }^\circ\text{C}$ , the CO production rate decreases due to an important decrease of the specific surface area. The CO production rate of nanostructured ceria was observed to be 6 times higher than for non-porous ceria,

with a reduction temperature of 1400 °C. It is similar to electrospun fibers under comparable operating conditions. Furthermore, the density of wood-templated ceria is higher than for fibers, allowing the loading of more reactive material. The performance stability of the wood-templated ceria was demonstrated by conducting 21 cycles [110].

To some extent, the advantages of nanostructured powders in terms of reactivity and kinetics can be constrained by some issues. Indeed, homogenous heating of the reactive powders is challenging and their processing in two-step cycles may require particle transport to carry out both reaction steps. Their use in solar thermochemical process requires the development of particle-based solar reactor technologies, such as fluidized bed, aerosol or entrained particle flow reactors, for efficient heat and mass transfer, but at the expense of additional particle transport between each cycle step and associated heat losses.

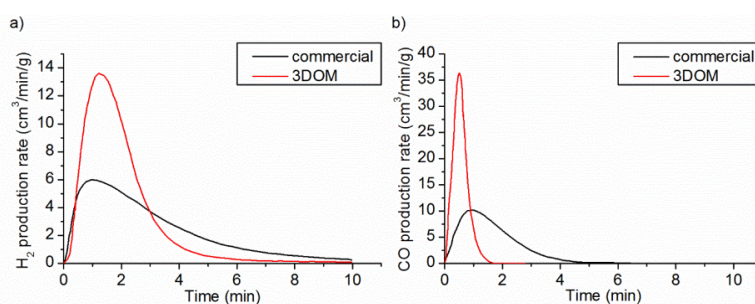


**Figure 7.** Comparison between 3DOM and commercial ceria powders for (a) H<sub>2</sub> production rate and (b) CO production rate, oxidation at 1100 °C [107].

In summary, the shaped materials should provide a good solar absorptivity favoring homogeneous heating, along with a high specific surface area favoring solid-gas reactions. A long-term thermal stability is also required for the considered ceria structures regardless of the involved shaping method. To achieve an economically viable solar fuel production, the enhancement of the thermochemical performance must be balanced with the additional cost caused by the materials shaping.

## 5. Conclusion

In the framework of the decarbonization of worldwide energy production, solar-driven thermochemical redox cycles represent a promising solution as solar energy is converted to solar fuels without CO<sub>2</sub> emission. Solar fuels can be stored, transported and used on-demand. Ceria is the benchmark material for thermochemical fuel production due its ability to produce oxygen vacancies while retaining its fluorite structure during reversible oxidation states, and its oxidation is thermodynamically favorable. Different studies investigated the thermodynamic and kinetic properties of ceria during thermochemical cycles. The oxygen non-stoichiometry reachable by ceria is the main issue limiting the fuel production yield. To enhance its overall reduction extent, numerous dopants were studied for improving oxygen mobility. The most promising are Zr<sup>4+</sup>, Hf<sup>4+</sup> and Sc<sup>3+</sup> cations and their incorporation is generally beneficial to the reduction step, by increasing

the reduction extent. However, it has generally a negative impact on the oxidation step, with a decrease of both the oxidation rate and the re-oxidation yield. The cation doping process requires carefully considering solubility, phase diagrams and phase stability. Another important parameter influencing the fuel production capability is the material shaping and design. Different morphologies including fibers, felts, nanostructured powders, and reticulated porous foams (with single and dual-scale porosity) have been considered in the literature. The fiber and felt materials have a high specific surface area that favors the oxidation step. Nevertheless, the solar absorption in the structure volume is low, yielding temperature gradients into the material and limiting the reduction step efficiency. On the contrary, reticulated porous foams with single-scale porosity (mm-pore size) show good solar radiation absorption, which favors the reduction step. However, their oxidation is limited due to the low specific surface area. To further improve the oxidation rate, micro-scale porosity has been introduced in reticulated porous foams (dual-scale foam) to increase the specific surface area while enabling volumetric solar radiation absorption. Nanostructured powders also exhibit a high specific surface area that promotes the oxidation step, but the nanostructure tends to be damaged at high temperatures. Moreover, the material shaping process represents an additional step required for the preparation of tailored materials and for their incorporation in suitable solar reactors, which could have an impact on the process economics. The design of optimized and thermally stable ceria structures with controlled morphologies and microstructures is thus a huge challenge for their large-scale implementation in high-temperature solar reactors applied to synthetic fuel production.

## Acknowledgments

This study was supported by the French National Agency for Research (ANR, SUNFUEL project, contract N °ANR-16-CE06-0010).

## Conflicts of interests

The authors declare no conflict of interests.

## References

1. Meredig B, Wolverton C (2009) First-principles thermodynamic framework for the evaluation of thermochemical H<sub>2</sub>O- or CO<sub>2</sub>-splitting materials. *Phys Rev B* 80: 245119.
2. Marxer D, Furler P, Takacs M, et al. (2017) Solar thermochemical splitting of CO<sub>2</sub> into separate streams of CO and O<sub>2</sub> with high selectivity, stability, conversion, and efficiency. *Energ Environ Sci* 10: 1142–1149.
3. Siegel NP, Miller JE, Ermanoski I, et al. (2013) Factors affecting the efficiency of solar driven metal oxide thermochemical cycles. *Ind Eng Chem Res* 52: 3276–3286.
4. Muhich CL, Ehrhart BD, Al-Shankiti I, et al. (2015) A review and perspective of efficient hydrogen generation via solar thermal water splitting. *WIREs Energy Environ* 5: 261–287.
5. Bhosale RR, Takalkar G, Sutar P, et al. (2019) A decade of ceria based solar thermochemical H<sub>2</sub>O/CO<sub>2</sub> splitting cycle. *Int J Hydrogen Energ* 44: 34–60.

6. McDaniel AH (2017) Renewable energy carriers derived from concentrating solar power and nonstoichiometric oxides. *Curr Opin Green Sustain Chem* 4: 37–43.
7. Furler P, Scheffe JR, Steinfeld A (2012) Syngas production by simultaneous splitting of H<sub>2</sub>O and CO<sub>2</sub> via ceria redox reactions in a high-temperature solar reactor. *Energ Environ Sci* 5: 6098–6103.
8. Haeussler A, Abanades S, Jouannaux J, et al. (2018) Non-stoichiometric redox active perovskite materials for solar thermochemical fuel production: a review. *Catalysts* 8: 611–631.
9. McDaniel AH, Miller EC, Arifin D, et al. (2013) Sr- and Mn-doped LaAlO<sub>3-δ</sub> for solar thermochemical H<sub>2</sub> and CO production. *Energ Environ Sci* 6: 2424–2428.
10. Scheffe JR, Weibel D, Steinfeld A (2013) Lanthanum-strontium-manganese perovskites as redox materials for solar thermochemical splitting of H<sub>2</sub>O and CO<sub>2</sub>. *Energ Fuel* 27: 4250–4257.
11. Demont A, Abanades S (2014) High redox activity of Sr-substituted lanthanum manganite perovskites for two-step thermochemical dissociation of CO<sub>2</sub>. *RSC Adv* 4: 54885–54891.
12. Demont A, Abanades S, Beche E (2014) Investigation of perovskite structures as oxygen-exchange redox materials for hydrogen production from thermochemical two-step water-splitting cycles. *J Phys Chem C* 118: 12682–12692.
13. McDaniel AH, Ambrosini A, Coker EN, et al. (2014) Nonstoichiometric perovskite oxides for solar thermochemical H<sub>2</sub> and CO production. *Energ Procedia* 49: 2009–2018.
14. Yang CK, Yamazaki Y, Aydın A, et al. (2014) Thermodynamic and kinetic assessments of strontium-doped lanthanum manganite perovskites for two-step thermochemical water splitting. *J Mater Chem A* 2: 13612–13623.
15. Deml AM, Stevanović V, Holder AM, et al. (2014) Tunable oxygen vacancy formation energetics in the complex perovskite oxide Sr<sub>x</sub>La<sub>1-x</sub>Mn<sub>y</sub>Al<sub>1-y</sub>O<sub>3</sub>. *Chem Mater* 26: 6595–6602.
16. Ezbiri M, Takacs M, Theiler D, et al. (2017) Tunable thermodynamic activity of La<sub>x</sub>Sr<sub>1-x</sub>Mn<sub>y</sub>Al<sub>1-y</sub>O<sub>3-δ</sub> (0 ≤ x ≤ 1, 0 ≤ y ≤ 1) perovskites for solar thermochemical fuel synthesis. *J Mater Chem A* 5: 4172–4182.
17. Demont A, Abanades S (2015) Solar thermochemical conversion of CO<sub>2</sub> into fuel via two-step redox cycling of non-stoichiometric Mn-containing perovskite oxides. *J Mater Chem A* 3: 3536–3546.
18. Ezbiri M, Allen KM, Gálvez ME, et al. (2015) Design principles of perovskites for thermochemical oxygen separation. *Chem Sus Chem* 8: 1966–1971.
19. Cooper T, Scheffe JR, Galvez ME, et al. (2015) Lanthanum manganite perovskites with Ca/Sr A-site and Al B-site doping as effective oxygen exchange materials for solar thermochemical fuel production. *Energy Technol* 3: 1130–1142.
20. Sastre D, Carrillo AJ, Serrano DP, et al. (2017) Exploring the redox behavior of La<sub>0.6</sub>Sr<sub>0.4</sub>Mn<sub>1-x</sub>Al<sub>x</sub>O<sub>3</sub> perovskites for CO<sub>2</sub>-splitting in thermochemical cycles. *Top Catal* 60: 1108–1118.

21. Barcellos DR, Sanders MD, Tong J, et al. (2018)  $\text{BaCe}_{0.25}\text{Mn}_{0.75}\text{O}_{3-\delta}$ —a promising perovskite-type oxide for solar thermochemical hydrogen production. *Energ Environ Sci* 11: 3256–3265.
22. Nair MM, Abanades S (2018) Experimental screening of perovskite oxides as efficient redox materials for solar thermochemical  $\text{CO}_2$  conversion. *Sustain Energ Fuels* 2: 843–854.
23. Wang L, Al-Mamun M, Liu P, et al. (2018) Notable hydrogen production on  $\text{La}_x\text{Ca}_{1-x}\text{CoO}_3$  perovskites via two-step thermochemical water splitting. *J Mater Sci* 53: 6796–6806.
24. Chen Z, Jiang Q, Cheng F, et al. (2019) Sr- and Co-doped  $\text{LaGaO}_{3-\delta}$  with high  $\text{O}_2$  and  $\text{H}_2$  yields in solar thermochemical water splitting. *J Mater Chem A* 7: 6099–6112.
25. Agrafiotis C, Roeb M, Sattler C (2015) A review on solar thermal syngas production via redox pair-based water/carbon dioxide splitting thermochemical cycles. *Renew Sust Energ Rev* 42: 254–285.
26. Kubicek M, Bork AH, Rupp JLM (2017) Perovskite oxides—a review on a versatile material class for solar-to-fuel conversion processes. *J Mater Chem A* 5: 11983–12000.
27. Sunarso J, Hashim SS, Zhu N, et al. (2017) Perovskite oxides applications in high temperature oxygen separation, solid oxide fuel cell and membrane reactor: a review. *Prog Energ Combust* 61: 57–77.
28. Kaneko H, Miura T, Ishihara H, et al. (2007) Reactive ceramics of  $\text{CeO}_2\text{—MO}_x$  ( $M = \text{Mn, Fe, Ni, Cu}$ ) for  $\text{H}_2$  generation by two-step water splitting using concentrated solar thermal energy. *Energy* 32: 656–663.
29. Andersson DA, Simak SI, Skorodumova NV, et al. (2007) Theoretical study of  $\text{CeO}_2$  doped with tetravalent ions. *Phys Rev B* 76: 174119.
30. Ackermann S, Sauvin L, Castiglioni R, et al. (2015) Kinetics of  $\text{CO}_2$  reduction over nonstoichiometric ceria. *J Phys Chem C* 119: 16452–16461.
31. Kaneko H, Ishihara H, Taku S, et al. (2008) Cerium ion redox system in  $\text{CeO}_{2-x}\text{Fe}_2\text{O}_3$  solid solution at high temperatures (1273–1673 K) in the two-step water-splitting reaction for solar  $\text{H}_2$  generation. *J Mater Sci* 43: 3153–3161.
32. Roeb M, Neises M, Monnerie N, et al. (2012) Materials-related aspects of thermochemical water and carbon dioxide splitting: a review. *Materials* 5: 2015–2054.
33. Montini T, Melchionna M, Monai M, et al. (2016) Fundamentals and catalytic applications of  $\text{CeO}_2$ -based materials. *Chem Rev* 116: 5987–6041.
34. Trovarelli A (1996) Catalytic properties of ceria and  $\text{CeO}_2$ -containing materials. *Catal Rev* 38: 439–520.
35. Bulfin B, Lowe AJ, Keogh KA, et al. (2013) Analytical model of  $\text{CeO}_2$  oxidation and reduction. *J Phys Chem C* 117: 24129–24137.
36. Bulfin B, Vieten J, Agrafiotis C, et al. (2017) Applications and limitations of two step metal oxide thermochemical redox cycles; a review. *J Mater Chem A* 5: 18951–18966.
37. Miller JE, McDaniel AH, Allendorf MD (2014) Considerations in the design of materials for solar-driven fuel production using metal-oxide thermochemical cycles. *Adv Energy Mater* 4: 1300469.
38. Abanades S, Flamant G (2006) Thermochemical hydrogen production from a two-step solar-driven water-splitting cycle based on cerium oxides. *Sol Energy* 80: 1611–1623.

39. Chueh WC, Haile SM (2009) Ceria as a thermochemical reaction medium for selectively generating syngas or methane from H<sub>2</sub>O and CO<sub>2</sub>. *ChemSusChem* 2: 735–739.
40. Chueh WC, Falter C, Abbott M, et al. (2010) High-flux solar-driven thermochemical dissociation of CO<sub>2</sub> and H<sub>2</sub>O using nonstoichiometric ceria. *Science* 330: 1797–1801.
41. Carrillo RJ, Scheffe JR (2017) Advances and trends in redox materials for solar thermochemical fuel production. *Sol Energy* 156: 3–20.
42. Scheffe JR, Steinfeld A (2014) Oxygen exchange materials for solar thermochemical splitting of H<sub>2</sub>O and CO<sub>2</sub>: a review. *Mater Today* 17: 341–348.
43. Chueh WC, Haile SM (2010) A thermochemical study of ceria: exploiting an old material for new modes of energy conversion and CO<sub>2</sub> mitigation. *Philos T Roy Soc A* 368: 3269–3294.
44. Rager T (2012) Re-evaluation of the efficiency of a ceria-based thermochemical cycle for solar fuel generation. *Chem Commun* 48: 10520–10522.
45. Rhodes NR, Bobek MM, Allen KM, et al. (2015) Investigation of long term reactive stability of ceria for use in solar thermochemical cycles. *Energy* 89: 924–931.
46. Ji HI, Davenport TC, Ignatowich MJ, et al. (2017) Gas-phase vs. material-kinetic limits on the redox response of nonstoichiometric oxides. *Phys Chem Chem Phys* 19: 7420–7430.
47. Furler P, Scheffe J, Marxer D, et al. (2014) Thermochemical CO<sub>2</sub> splitting via redox cycling of ceria reticulated foam structures with dual-scale porosities. *Phys Chem Chem Phys* 16: 10503–10511.
48. Farooqui AE, Pica AM, Marocco P, et al. (2018) Assessment of kinetic model for ceria oxidation for chemical-looping CO<sub>2</sub> dissociation. *Chem Eng J* 346: 171–181.
49. Arifin D, Weimer AW (2018) Kinetics and mechanism of solar-thermochemical H<sub>2</sub> and CO production by oxidation of reduced CeO<sub>2</sub>. *Sol Energy* 160: 178–185.
50. Ackermann S, Scheffe JR, Steinfeld A (2014) Diffusion of oxygen in ceria at elevated temperatures and its application to H<sub>2</sub>O/CO<sub>2</sub> splitting thermochemical redox cycles. *J Phys Chem C* 118: 5216–5225.
51. Davenport TC, Yang CK, Kucharczyk CJ, et al. (2016) Maximizing fuel production rates in isothermal solar thermochemical fuel production. *Appl Energy* 183: 1098–1111.
52. Bader R, Venstrom LJ, Davidson JH, et al. (2013) Thermodynamic analysis of isothermal redox cycling of ceria for solar fuel production. *Energy Fuel* 27: 5533–5544.
53. Meng QL, Lee C, Ishihara T, et al. (2011) Reactivity of CeO<sub>2</sub>-based ceramics for solar hydrogen production via a two-step water-splitting cycle with concentrated solar energy. *Int J Hydrogen Energy* 36: 13435–13441.
54. Meng QL, Lee C, Shigeta S, et al. (2012) Solar hydrogen production using Ce<sub>1-x</sub>Li<sub>x</sub>O<sub>2-δ</sub> solid solutions via a thermochemical, two-step water-splitting cycle. *J Solid State Chem* 194: 343–351.
55. Scheffe JR, Steinfeld A (2012) Thermodynamic analysis of cerium-based oxides for solar thermochemical fuel production. *Energy Fuel* 26: 1928–1936.
56. Muhich C, Steinfeld A (2017) Principles of doping ceria for the solar thermochemical redox splitting of H<sub>2</sub>O and CO<sub>2</sub>. *J Mater Chem A* 5: 15578–15590.

57. Jaiswal N, Kumar D, Upadhyay S, et al. (2013) Effect of Mg and Sr co-doping on the electrical properties of ceria-based electrolyte materials for intermediate temperature solid oxide fuel cells. *J Alloy Compd* 577: 456–462.
58. Scheffe JR, Jacot R, Patzke GR, et al. (2013) Synthesis, characterization, and thermochemical redox performance of Hf<sup>4+</sup>, Zr<sup>4+</sup>, and Sc<sup>3+</sup> doped ceria for splitting CO<sub>2</sub>. *J Phys Chem C* 117: 24104–24114.
59. Lee C, Meng QL, Kaneko H, et al. (2012) Solar hydrogen productivity of ceria-scandia solid solution using two-step water-splitting cycle. *J Sol Energ-T Asme* 135: 011002–011008.
60. Jiang Q, Zhou G, Jiang Z, et al. (2014) Thermochemical CO<sub>2</sub> splitting reaction with Ce<sub>x</sub>M<sub>1-x</sub>O<sub>2-δ</sub> (M = Ti<sup>4+</sup>, Sn<sup>4+</sup>, Hf<sup>4+</sup>, Zr<sup>4+</sup>, La<sup>3+</sup>, Y<sup>3+</sup> and Sm<sup>3+</sup>) solid solutions. *Sol Energy* 99: 55–66.
61. Ramos-Fernandez EV, Shiju NR, Rothenberg G (2014) Understanding the solar-driven reduction of CO<sub>2</sub> on doped ceria. *RSC Adv* 4: 16456–16463.
62. Gokon N, Suda T, Kodama T (2015) Oxygen and hydrogen productivities and repeatable reactivity of 30-mol%-Fe-, Co-, Ni-, Mn-doped CeO<sub>2-δ</sub> for thermochemical two-step water-splitting cycle. *Energy* 90: 1280–1289.
63. Le Gal A, Abanades S (2012) Dopant Incorporation in ceria for enhanced water-splitting activity during solar thermochemical hydrogen generation. *J Phys Chem C* 116: 13516–13523.
64. Bhosale RR, Takalkar GD (2018) Nanostructured co-precipitated Ce<sub>0.9</sub>Ln<sub>0.1</sub>O<sub>2</sub> (Ln = La, Pr, Sm, Nd, Gd, Tb, Dy, or Er) for thermochemical conversion of CO<sub>2</sub>. *Ceram Int* 44: 16688–16697.
65. Meng QL, Lee CI, Kaneko H, et al. (2012) Solar thermochemical process for hydrogen production via two-step water splitting cycle based on Ce<sub>1-x</sub>Pr<sub>x</sub>O<sub>2-δ</sub> redox reaction. *Thermochim Acta* 532: 134–138.
66. Jacot R, Moré R, Michalsky R, et al. (2017) Trends in the phase stability and thermochemical oxygen exchange of ceria doped with potentially tetravalent metals. *J Mater Chem A* 5: 19901–19913.
67. Bonk A, Maier AC, Schlupp MVF, et al. (2015) The effect of dopants on the redox performance, microstructure and phase formation of ceria. *J Power Sources* 300: 261–271.
68. Montini T, Hickey N, Fornasiero P, et al. (2005) Variations in the extent of pyrochlore-type cation ordering in Ce<sub>2</sub>Zr<sub>2</sub>O<sub>8</sub>: a t<sup>-</sup>-k pathway to low-temperature reduction. *Chem Mater* 17: 1157–1166.
69. Tani E, Yoshimura M, Somiya S (1983) Revised phase diagram of the system ZrO<sub>2</sub>–CeO<sub>2</sub> below 1400 °C. *J Am Ceram Soc* 66: 506–510.
70. Thomson JB, Armstrong AR, Bruce PG (1996) A new class of pyrochlore solid solution formed by chemical intercalation of oxygen. *J Am Chem Soc* 118: 11129–11133.
71. Montini T, Bañares MA, Hickey N, et al. (2004) Promotion of reduction in Ce<sub>0.5</sub>Zr<sub>0.5</sub>O<sub>2</sub>: the pyrochlore structure as effect rather than cause? *Phys Chem Chem Phys* 6: 1–3.
72. Abanades S, Legal A, Cordier A, et al. (2010) Investigation of reactive cerium-based oxides for H<sub>2</sub> production by thermochemical two-step water-splitting. *J Mater Sci* 45: 4163–4173.

73. Abanades S, Le Gal A (2012) CO<sub>2</sub> splitting by thermo-chemical looping based on Zr<sub>x</sub>Ce<sub>1-x</sub>O<sub>2</sub> oxygen carriers for synthetic fuel generation. *Fuel* 102: 180–186.
74. Takacs M, Scheffe JR, Steinfeld A (2015) Oxygen nonstoichiometry and thermodynamic characterization of Zr doped ceria in the 1573–1773 K temperature range. *Phys Chem Chem Phys* 17: 7813–7822.
75. Le Gal A, Abanades S, Bion N, et al. (2013) Reactivity of doped ceria-based mixed oxides for solar thermochemical hydrogen generation via two-step water-splitting cycles. *Energ Fuel* 27: 6068–6078.
76. Fornasiero P, Dimonte R, Rao GR, et al. (1995) Rh-loaded CeO<sub>2</sub>–ZrO<sub>2</sub> solid-solutions as highly efficient oxygen exchangers: dependence of the reduction behavior and the oxygen storage capacity on the structural-properties. *J Catal* 151: 168–177.
77. Le Gal A, Abanades S (2011) Catalytic investigation of ceria-zirconia solid solutions for solar hydrogen production. *Int J Hydrogen Energy* 36: 4739–4748.
78. Vlaic G, Fornasiero P, Geremia S, et al. (1997) Relationship between the Zirconia-promoted reduction in the Rh-loaded Ce<sub>0.5</sub>Zr<sub>0.5</sub>O<sub>2</sub> mixed oxide and the Zr–O local structure. *J Catal* 168: 386–392.
79. Yang Z, Woo TK, Hermansson K (2006) Effects of Zr doping on stoichiometric and reduced ceria: a first-principles study. *J Chem Phys* 124: 224704.
80. Esch F (2005) Electron localization determines defect formation on ceria substrates. *Science* 309: 752–755.
81. Shah PR, Kim T, Zhou G, et al. (2006) Evidence for entropy effects in the reduction of ceria-zirconia solutions. *Chem Mater* 18: 5363–5369.
82. Muhich C, Hoes M, Steinfeld A (2018) Mimicking tetravalent dopant behavior using paired charge compensating dopants to improve the redox performance of ceria for thermochemically splitting H<sub>2</sub>O and CO<sub>2</sub>. *Acta Mater* 144: 728–737.
83. Bulfin B, Lange M, de Oliveira L, et al. (2016) Solar thermochemical hydrogen production using ceria zirconia solid solutions: efficiency analysis. *Int J Hydrogen Energy* 41: 19320–19328.
84. Ganzoury MA, Fateen SEK, El Sheltawy ST, et al. (2016) Thermodynamic and efficiency analysis of solar thermochemical water splitting using Ce–Zr mixtures. *Sol Energy* 135: 154–162.
85. Le Gal A, Abanades S, Flamant G (2011) CO<sub>2</sub> and H<sub>2</sub>O splitting for thermochemical production of solar fuels using nonstoichiometric ceria and ceria/zirconia solid solutions. *Energ Fuel* 25: 4836–4845.
86. Muhich CL, Blaser S, Hoes MC, et al. (2018) Comparing the solar-to-fuel energy conversion efficiency of ceria and perovskite based thermochemical redox cycles for splitting H<sub>2</sub>O and CO<sub>2</sub>. *Int J Hydrogen Energy* 43: 18814–18831.
87. Call F, Roeb M, Schmücker M, et al. (2015) Ceria doped with zirconium and lanthanide oxides to enhance solar thermochemical production of fuels. *J Phys Chem C* 119: 6929–6938.
88. Kang M, Zhang J, Wang C, et al. (2013) CO<sub>2</sub> splitting via two step thermochemical reactions over doped ceria/zirconia solid solutions. *RSC Adv* 3: 18878–18885.

89. Kang M, Wu X, Zhang J, et al. (2014) Enhanced thermochemical CO<sub>2</sub> splitting over Mg- and Ca-doped ceria/zirconia solid solutions. *RSC Adv* 4: 5583–5590.
90. Bhosale RR, Kumar A, AlMomeni F, et al. (2016) Assessment of Ce<sub>x</sub>Zr<sub>y</sub>Hf<sub>z</sub>O<sub>2</sub> based oxides as potential solar thermochemical CO<sub>2</sub> splitting materials. *Ceram Int* 42: 9354–9362.
91. Jacot R, Naik JM, MoréR, et al. (2018) Reactive stability of promising scalable doped ceria materials for thermochemical two-step CO<sub>2</sub> dissociation. *J Mater Chem A* 6: 5807–5816.
92. Meng QL, Tamaura Y (2014) Enhanced hydrogen production by doping Pr into Ce<sub>0.9</sub>Hf<sub>0.1</sub>O<sub>2</sub> for thermochemical two-step water-splitting cycle. *J Phys Chem Solids* 75: 328–333.
93. Ruan C, Tan Y, Li L, et al. (2017) A novel CeO<sub>2-x</sub>SnO<sub>2</sub>/Ce<sub>2</sub>Sn<sub>2</sub>O<sub>7</sub> pyrochlore cycle for enhanced solar thermochemical water splitting. *AIChE J* 63: 3450–3462.
94. Lin F, Wokaun A, Alxneit I (2015) Rh-doped ceria: solar organics from H<sub>2</sub>O, CO<sub>2</sub> and sunlight? *Energy Procedia* 69: 1790–1799.
95. Mostrou S, Büchel R, Pratsinis SE, et al. (2017) Improving the ceria-mediated water and carbon dioxide splitting through the addition of chromium. *Appl Catal A* 537: 40–49.
96. Hoes M, Muhich CL, Jacot R, et al. (2017) Thermodynamics of paired charge-compensating doped ceria with superior redox performance for solar thermochemical splitting of H<sub>2</sub>O and CO<sub>2</sub>. *J Mater Chem A* 5: 19476–19484.
97. Kaneko H, Tamaura Y. (2009) Reactivity and XAFS study on (1 - x)CeO<sub>2-x</sub>NiO (x = 0.025–0.3) system in the two-step water-splitting reaction for solar H<sub>2</sub> production. *J Phys Chem Solids* 70: 1008–1014.
98. Lin F, Samson VA, Wismer AO, et al. (2016) Zn-modified ceria as a redox material for thermochemical H<sub>2</sub>O and CO<sub>2</sub> splitting: effect of a secondary ZnO phase on its thermochemical activity. *CrystEngComm* 18: 2559–2569.
99. Yadav D, Banerjee R (2016) A review of solar thermochemical processes. *Renew Sustain Energ Rev* 54: 497–532.
100. Gibbons WT, Venstrom LJ, De Smith RM, et al. (2014) Ceria-based electrospun fibers for renewable fuel production via two-step thermal redox cycles for carbon dioxide splitting. *Phys Chem Chem Phys* 16: 14271–14280.
101. Gladen AC, Davidson JH (2016) The morphological stability and fuel production of commercial fibrous ceria particles for solar thermochemical redox cycling. *Sol Energy* 139: 524–532.
102. Furler P, Scheffe J, Gorbar M, et al. (2012) Solar thermochemical CO<sub>2</sub> splitting utilizing a reticulated porous ceria redox system. *Energy Fuel* 26: 7051–7059.
103. Takacs M, Ackermann S, Bonk A, et al. (2017) Splitting CO<sub>2</sub> with a ceria-based redox cycle in a solar-driven thermogravimetric analyzer. *AIChE J* 63: 1263–1271.
104. Cho HS, Myojin T, Kawakami S, et al. (2014) Solar demonstration of thermochemical two-step water splitting cycle using CeO<sub>2</sub>/MPSZ ceramic foam device by 45kW<sub>th</sub> KIER solar furnace. *Energy Procedia* 49: 1922–1931.
105. Ackermann S, Scheffe J, Duss J, et al. (2014) Morphological characterization and effective thermal conductivity of dual-scale reticulated porous structures. *Materials* 7: 7173–7195.

106. Marxer D, Furler P, Scheffe J, et al. (2015) Demonstration of the entire production chain to renewable kerosene via solar thermochemical splitting of H<sub>2</sub>O and CO<sub>2</sub>. *Energ Fuel* 29: 3241–3250.
107. Venstrom LJ, Petkovich N, Rudisill S, et al. (2012) The effects of morphology on the oxidation of ceria by water and carbon dioxide. *J Sol Energ Eng* 134: 011005–011012.
108. Petkovich ND, Rudisill SG, Venstrom LJ, et al. (2011) Control of heterogeneity in nanostructured Ce<sub>1-x</sub>Zr<sub>x</sub>O<sub>2</sub> binary oxides for enhanced thermal stability and water splitting activity. *J Phys Chem C* 115: 21022–21033.
109. Oliveira FAC, Barreiros MA, Abanades S, et al. (2018) Solar thermochemical CO<sub>2</sub> splitting using cork-templated ceria ecoceramics. *J CO<sub>2</sub> Util* 26: 552–563.
110. Malonzo CD, De Smith RM, Rudisill SG, et al. (2014) Wood-templated CeO<sub>2</sub> as active material for thermochemical CO production. *J Phys Chem C* 118: 26172–26181.



AIMS Press

© 2019 the Author(s), licensee AIMS Press. This is an open access article distributed under the terms of the Creative Commons Attribution License (<http://creativecommons.org/licenses/by/4.0>)